PAPER

Statistical theory for the reaction N + OH → NO + H: thermal low-temperature rate constants

A. I. Maergoiz, [ID] [ab] E. E. Nikitin[ac] and J. Troe [ID] *[ab]

The reaction N + OH → NO + H involves the intermediate formation of NOH adducts which in part rearrange to HNO conformers. A statistical treatment of the process is developed in which an initial adiabatic channel capture of the reactants is accompanied by partial primary redissociation of the N···OH collision pairs. A criterion for the extent of this primary redissociation in competition to the formation of randomized, long-lived, complex of NOH is proposed. The NOH adducts then may decompose to NO + H, rearrange in a unimolecular process to HNO, or undergo secondary redissociation back to the reactants N + OH, while HNO may also decompose to NO + H. As the reactants $N(^4S)$ + $OH(^2\Pi)$ have open electronic shells, non-Born–Oppenheimer effects have to be considered. Their influence on thermal rate constants of the reaction at low temperatures is illustrated and compared with such effects in other reactions such as $C(^3P)$ + $OH(^2\Pi)$.

1. Introduction

The mechanism of complex-forming bimolecular reactions can be understood in terms of an initial capture of the reactants, the formation of long-lived adducts, and the subsequent decay of these adducts. While adiabatic capture theory often characterizes the initial stage of the reaction, statistical unimolecular rate theory is frequently used to quantify the intramolecular evolution of the adducts. The described concept has successfully rationalized a large number of experimental results. Simplified versions of the treatment have been proposed, for instance, in ref. 1. Looking into the finer details of the reaction, however, a number of aspects deserve further attention.

(i) Obviously, the potential energy surface (PES) of the system plays a central role. The identification and proper representation of the rate-determining parts of the PES, therefore, is of high priority.

[a]Max-Planck-Institut für Multidisziplinäre Naturwissenschaften, Am Fassberg 11, D-37077 Göttingen, Germany. E-mail: juergen.troe@mpinat.mpg.de

[b]Institut für Physikalische Chemie, Universität Göttingen, Tammannstr. 6, D-37077 Göttingen, Germany

[c]Schulich Faculty of Chemistry, Technion-Israel Institute of Technology, Haifa 32000, Israel

(ii) The reactants may have open electronic shells and the interaction between the arising PESs has to be taken into account. This complicates the analysis on the Born–Oppenheimer (BO) level of the interaction between individual adiabatic channel potential energy curves, see, for instance, the capture of C(^{3}P) by OH($^2\Pi$) elaborated in ref. 2, or the capture of H(^{2}S) by O$_2$($^3\Sigma$) and of O(^{3}P) by OH($^2\Pi$) discussed in ref. 3. It is common practice to consider reaction on a single PES, which correlates with a single state of the reactants, and to multiply the resulting thermal rate constants by electronic factors $f_{el}(T)$ which account for the thermal population of the reactants in their relevant fine-structure levels.[4] Because of the interaction of the PESs at large intermolecular distances, this may not be sufficient for low-temperature conditions; but as the consequences may reach up to temperatures of several tens of K, they may be important for astrochemical applications, for instance, see ref. 5 and 6.

(iii) Reaction cross sections and thermal rate constants for capture from the statistical adiabatic channel model (SACM, ref. 7 and 8), have been compared with results from quasi-classical trajectory (CT) calculations in ref. 9–13. The extent of dynamical non-adiabaticity was inspected and simplified representations of the SACM/CT results were proposed. While quantum effects of the internal reactant states are accounted for in SACM/CT approaches from the beginning, comparisons with detailed quantum scattering (CS) calculations are also required, in particular when capture of light particles like electrons are considered, for instance, see ref. 14.

(iv) The connection of the initial capture of the reactants with the subsequent evolution of the adduct may be of importance and has to be understood on a state-specific level. There may be "primary redissociation" of the "collision pair", before a long-lived complex is formed. At a later stage of the process, a "secondary (unimolecular) redissociation" of the randomized adduct may take place in competition to other decay channels. Both types of redissociation lead to a reduction of the reaction rate in comparison to the capture rate.

It is the aim of the present work to illustrate the described details of an analysis within an extended SACM approach. The complex-forming, exothermic, bimolecular reaction

$$N(^4S) + OH(^2\Pi) \rightarrow (NOH, HNO) \rightarrow H(^2S) + NO(^2\Pi) \quad \Delta H_0^\circ = -201.1 \text{ kJ mol}^{-1}$$

(1)
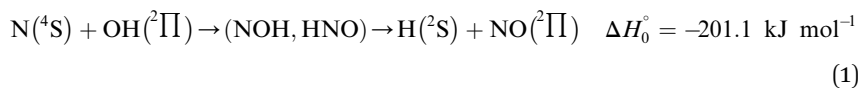
is chosen as an example, because extensive previous work is available for this system and allows for a validation of the proposed treatment. For instance, *ab initio* calculations of the PES, including that part which is responsible for the intermediate change of conformation NOH → HNO, have been made (for instance, see ref. 15–20). Rate constants for the capture process have been estimated before, by applying a simplified SACM[21] or an adiabatic capture centrifugal sudden approximation (ACCSA).[22,23] Detailed CT calculations of state-resolved dynamics on a BO PES have been reported in ref. 24–26, while explicit QS calculations have been described in ref. 19 and 27–29. Product energy distributions and state-to-state reaction cross sections from these studies are particularly helpful for a validation of the respective treatments. Thermal rate constants on the relevant PES in the mentioned studies were combined with electronic state population factors $f_{el}(T)$ and then compared with experimental rate constants.[30–33]

Considerable differences between earlier and later experimental results have been overcome by the more recent work in ref. 6 and 33. The present study aims for rate constants at low temperatures, comparing $f_{el}(T)$-corrected BO with non-BO (NBO) calculations.

The comparison of experimental and modelled rate constants for reaction (1) leads to interesting conclusions. Like in ref. 23 one realizes that modelled capture rate constants are markedly higher than the experimental low-temperature values of the reaction rate constants from ref. 6 and 33, corresponding to probabilities for reaction after capture of only about 1/2. Similar values in ref. 23 were found for the reactions of O, S, and N atoms with OH. As ACCSA and SACM calculations for the same PES are essentially equivalent (for instance, see ref. 34), the present work is in agreement with this result. On the other hand, ACCSA, SACM, and CT calculations led to practically identical rate constants for the reaction of C with OH which corresponds to probabilities for reaction after capture near unity. Likewise, ACCSA and SACM calculations of capture rate constants were found to agree with experimental data for reactions of N^+ ions with H_2O or NH_3.[35]

The conclusion on probabilities smaller than unity for reaction after capture calls for an explanation. This may be found in CT calculations, such as those performed for reaction (1) in ref. 24, or for the reaction of O with OH in ref. 36–38. "Recrossing effects" then may be distinguished in terms of "primary redissociation" and/or "secondary redissociation" mechanisms of the initial collision pairs of reactants and of the adducts being formed, respectively. In the present work, we propose to characterize the redissociation processes by a state-specific criterion. We consider various factors possibly leading to primary redissociation, such as the number of atoms in the reactants, the distribution of masses between the reactants, the properties of the PES, and NBO effects under low-temperature conditions. Tests for the validity of the proposed approach are made by comparing modelled and experimental reaction rate constants. When the latter are not available, comparisons of rate constants for reaction from the present approach and from CT calculations are also useful. Finally, comparisons of product state distributions from the present approach and from CT calculations are helpful. This will be demonstrated for reaction (1) in the present article as well as in the more detailed publications of ref. 39 and 40.

2. Potential energy surfaces for the capture/redissociation process $N(^4S) + OH(^2\Pi) \leftrightarrow N\cdots OH$

An energy diagram for the intermediates of reaction (1) on the attractive $^3A''$ PES of the reaction system is shown in Fig. 1 (adapted from ref. 19, scaled with energies for N + OH, NOH, HNO, and H + NO from ref. 41; the species NOH, HNO, and the various transition states correspond to different structures on the same PES). Instead of the *ab initio* characterization of the PES performed in ref. 15–20, the present work determined part of the PES by the asymptotic method described in ref. 2, 3, 23 and 42. Furthermore, it focuses attention on the entrance side of the PES, *i.e.* on the side of the reactants N + OH, while the remaining parts, relevant for the transformation NOH $\leftrightarrow$ HNO and the subsequent dissociation (NOH, HNO) $\rightarrow$ H(^2S) + NO($^2\Pi$), will be elaborated in ref. 39 and 40. An asymptotic long-range potential between N(^4S) and OH($^2\Pi$), considering dispersion and induction
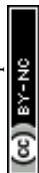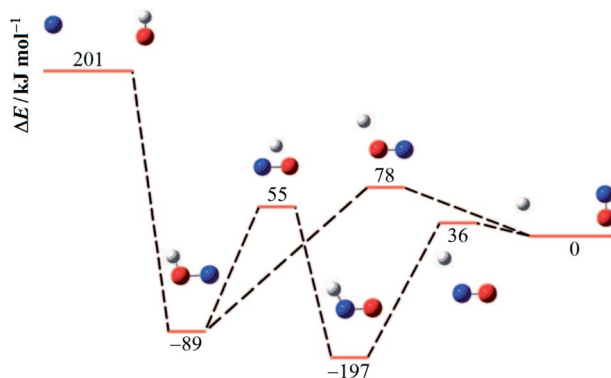
Fig. 1 Energy diagram for reaction (1) and its intermediates (blue, red, and white spheres symbolize N, O, and H atoms, respectively; the energies ΔE relative to H + NO are adapted from ref. 19 and 41).

interactions, but neglecting exchange interaction, has been constructed before,[23] the present work in this respect goes beyond this. In addition, we also go beyond the BO approximation. The treatment closely follows the procedure described in more detail in ref. 2. It also uses the nomenclature from that article.

In order to construct asymptotic PESs within the BO approximation, following ref. 2 we use a basis of electronic functions of the system with total spin $S = 1, 2$ in the form

$$\psi_{\pm}^{\text{el}} = \langle L, M_{\text{L}}, \Lambda, S, M_{\text{S}}| = \langle L=0, M_{\text{L}}=0|\langle \Lambda = \pm 1|\langle S, M_{\text{S}}| \quad (2)$$

($L = 0$ and $M_{\text{L}} = 0$ correspond to the electronic moment of ground state N atoms and its projection onto the N–OH axis, Λ denotes the projection of the electronic moment of a hypothetical spin–orbit (SO) structureless ground state of OH on its molecular axis). In asymptotic theory, diagonalization of the total interaction matrices $\hat{U}_{\text{S}}^{\text{ex}} + \hat{U}^{\text{ind}} + \hat{U}^{\text{disp}}$ generates four PESs (the SO interaction originating from OH($^2\Pi$) is neglected here; we note that there is no SO structure in N(^{4}S)). The four PESs correspond to $^3\text{A}', ^3\text{A}'', ^5\text{A}', ^5\text{A}''$ classification, of which only the $^3\text{A}''$ PES is attractive and eventually reactive, while the other PESs are repulsive and considered nonreactive in the energy range of interest. On the basis of the electronic wave functions of eqn (2), the matrix elements of the sum of the induction and dispersion interactions are

$$\langle L = 0, M_{\text{L}} = 0, S, M_{\text{S}}, \Lambda |U^{\text{ind}} + U^{\text{disp}}|L = 0, M_{\text{L}}' = 0, S, M_{\text{S}}, \Lambda' \rangle$$
$$= -R^{-6} \sum_{L_{\text{b}}, M_{\text{a}}, M_{\text{b}}} \left({}^{\text{ind}}V_{6, L_{\text{b}} M_{\text{a}} M_{\text{b}}}^{M_{\text{L}} M_{\text{L}}', \Lambda\Lambda'} + {}^{\text{disp}}V_{6, L_{\text{b}} M_{\text{a}} M_{\text{b}}}^{M_{\text{L}} M_{\text{L}}', \Lambda\Lambda'} \right) d_{-M_{\text{a}}, M_{\text{b}}}^{L_{\text{b}}}(\theta) \quad (3)$$

(with $M_{\text{a}} = 0$, $M_{\text{b}} = \Lambda - \Lambda'$; unless stated differently, energies are in atomic units 27.2116 eV = 2625.5 kJ mol^{-1} and distances in units of $a_0 = 0.52918 \times 10^{-8}$ cm). R and θ are the Jacobi coordinates of the N–OH system (distance and angle between the OH and N–OH axes, respectively). State-specific coefficients ${}^{\text{ind}}V_{6, L_{\text{b}} M_{\text{a}} M_{\text{b}}}^{M_{\text{L}} M_{\text{L}}', \Lambda\Lambda'}$ and ${}^{\text{disp}}V_{6, L_{\text{b}} M_{\text{a}} M_{\text{b}}}^{M_{\text{L}} M_{\text{L}}', \Lambda\Lambda'}$, are induction and dispersion coefficients, respectively, and are

Faraday Discussions

Table 1 State-specific coefficients for induction and dispersion matrix elements in eqn (3) (see also ref. 23)

M_L	M_L'	Λ, Λ'	L_b	M_a	M_b	${}^{\text{ind}}V_{6,L_b M_a M_b}^{M_L M_L', \Lambda \Lambda'}$
0	0	$\pm 1, \pm 1$	0	0	0	3.119
0	0	$\pm 1, \pm 1$	2	0	0	3.119

M_L	M_L'	Λ, Λ'	L_b	M_a	M_b	${}^{\text{disp}}V_{6,L_b M_a M_b}^{M_L M_L', \Lambda \Lambda'}$
0	0	$\pm 1, \pm 1$	0	0	0	32.163
0	0	$\pm 1, \pm 1$	2	0	0	2.157
0	0	$\pm 1, \pm 1$	2	0	± 2	-0.992

given in Table 1, in agreement with those from ref. 23. Composed from these elements, one has the matrix $\hat{U}^{\text{ind}} + \hat{U}^{\text{disp}}$ in the form

$$\hat{U}^{\text{ind}} + \hat{U}^{\text{disp}} = \begin{pmatrix} a & b \\ b & a \end{pmatrix}$$

$$\text{with } a = -\{35.283 + 2.638[3\cos^2(\theta) - 1]\}/R^6$$
$$b = 0.405\{1 + 2[3\cos^2(\theta) - 1]\}/R^6$$

(4)

Using the same basis as eqn (2), the exchange interaction matrix is given by

$$\hat{U}_S^{\text{ex}} = \begin{pmatrix} c_S & d_S \\ d_S & c_S \end{pmatrix}, \quad c_S = c_1 + \delta c, \quad d_S = d_1 + \delta d$$

with

$$c_1 = \left\{ \frac{RI_{00}^{(1,2)}}{3} - \frac{2I_{11}^{(1,2)}}{3\mu_{(1,2)}} - \frac{2I_{1-1}^{(1,4)}}{3\mu_{(1,4)}} + \frac{4I_{1-1}^{(1,4)}}{3R}\left(2 + \frac{1}{\mu_{(1,4)}} + \frac{1}{\mu_{(1,4)}^2}\right) \right.$$

$$\left. + \frac{3RI_{00}^{(3,2)}}{4} - \frac{3I_{1-1}^{(3,4)}}{2\mu_{(3,4)}} \right\}\sin^2\theta + \left\{ \frac{2RI_{00}^{(1,4)}}{3} - \frac{4I_{11}^{(1,4)}}{3\mu_{(1,4)}} + \frac{3RI_{00}^{(3,4)}}{2} \right\}\cos^2\theta$$

$$+ \left\{ -\frac{I_{1-1}^{(1,2)}}{3\mu_{(1,2)}} + \frac{2I_{20}^{(1,2)}}{3R}\left(2 + \frac{1}{\mu_{(1,2)}} + \frac{1}{\mu_{(1,2)}^2}\right) - \frac{3I_{1-1}^{(3,2)}}{4\mu_{(3,2)}} \right\}(1 + \cos^2\theta),$$

$$d_1 = \left\{ \frac{RI_{00}^{(1,2)}}{3} - \frac{4I_{11}^{(1,2)}}{3\mu_{(1,2)}} + \frac{2I_{1-1}^{(1,2)}}{3\mu_{(1,2)}} - \frac{4I_{20}^{(1,2)}}{3R}\left(2 + \frac{1}{\mu_{(1,2)}} + \frac{1}{\mu_{(1,2)}^2}\right) \right.$$

$$\left. + \frac{RI_{00}^{(3,2)}}{4} + \frac{RI_{1-1}^{(3,2)}}{4\mu_{(3,2)}} \right\}\sin^2\theta,$$

$$\delta c = \left\{ \frac{2RI_{00}^{(1,2)}}{3} - \frac{4I_{11}^{(1,2)}}{3\mu_{(1,2)}} \right\} \sin^2 \theta + \left\{ -\frac{2I_{1-1}^{(1,2)}}{3\mu_{(1,2)}} + \frac{4I_{20}^{(1,2)}}{3R} \left(2 + \frac{1}{\mu_{(1,2)}} + \frac{1}{\mu_{(1,2)}^2} \right) \right\}$$
$$\times (1 + \cos^2 \theta),$$

$$\delta d = \left\{ -\frac{2RI_{00}^{(1,2)}}{3} + \frac{4I_{11}^{(1,2)}}{3\mu_{(1,2)}} - \frac{2I_{1-1}^{(1,2)}}{3\mu_{(1,2)}} + \frac{4I_{20}^{(1,2)}}{3R} \left(2 + \frac{1}{\mu_{(1,2)}} + \frac{1}{\mu_{(1,2)}^2} \right) \right\} \sin^2 \theta \quad (5)$$

(It is assumed that the center of mass of OH approximately coincides with the position of the O atom.) Following ref. 2 and 42, the sums of the orbital exponents $\mu_{(q,q')} = \gamma_q + \gamma_{q'}$ and the preexponential factors A_q of the asymptotic orbital wave functions (corresponding to eqn (2.13) from ref. 2) were calculated as given in Table 2, while the exchange integrals of the orbitals $I_{kn}^{(q,q')}$ (corresponding to eqn (2.15) from ref. 2), for $R > 5a_0$, were expressed by

$$\ln(I_{kn}^{(q,q')}) = a_{kn}^{(q,q')}R^3 + b_{kn}^{(q,q')}R^2 + c_{kn}^{(q,q')}R + d_{kn}^{(q,q')} \quad (6)$$

with fitted coefficients such as those given in Table 3.

Combining the induction, dispersion, and exchange terms on the side of the reactants N + OH, for the $^3A', ^3A'', ^5A', ^5A''$ states one obtains

Table 2 Parameters of the asymptotic orbital wave functions (corresponding to eqn (2.13) of ref. 2)

q	Orbitals	γ_q	A_q
1	N,2p	1.0336	1.6
2	OH,1π	0.9775	1.6
3	N,2s	1.2225	2.0
4	OH,3σ	1.1012	2.0

Table 3 Fitting coefficients for the exchange integrals in eqn (6) (corresponding to eqn (2.15) of ref. 2)

| q	q'	k	n	$100a_{kn}^{(q,q')}$	$10b_{kn}^{(q,q')}$	$c_{kn}^{(q,q')}$	$d_{kn}^{(q,q')}$
1	2	0	0	0.1463	−0.4572	−1.3693	1.2581
1	2	1	0	0.1463	−0.4572	−1.3695	0.5592
1	2	1	1	0.1462	−0.4578	−1.3455	1.1455
1	2	1	−1	0.1464	−0.4578	−1.3934	1.0879
1	2	2	0	0.1463	−0.4572	−1.3698	−0.1396
1	4	0	0	0.1264	−0.3934	−1.5797	1.7100
1	4	1	0	0.1264	−0.3934	−1.5801	0.9513
1	4	1	1	0.1267	−0.3944	−1.6097	1.5027
1	4	1	−1	0.1263	−0.3944	−1.5500	1.5636
1	4	2	0	0.1264	−0.3934	−1.5804	0.1928
3	2	0	0	0.1124	−0.3195	−1.6589	1.6961
3	2	1	−1	0.1222	−0.3254	−1.7752	1.4014
3	4	0	0	0.1000	−0.3021	−1.8799	2.1609
3	4	1	−1	0.1017	−0.3056	−1.9364	1.8899
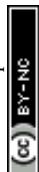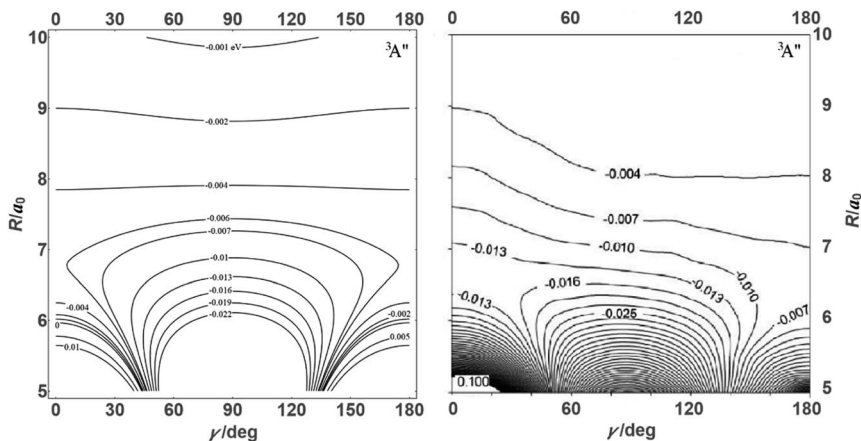
Fig. 2 Energy contours (in eV) of the attractive $^3A''$ PES of the N + OH system (Jacobi coordinates: N−OH distances R in atomic units, $\gamma = \theta$ in degrees). Comparison of results from the present asymptotic theory (left) with results from the *ab initio* calculations of ref. 19 (right).
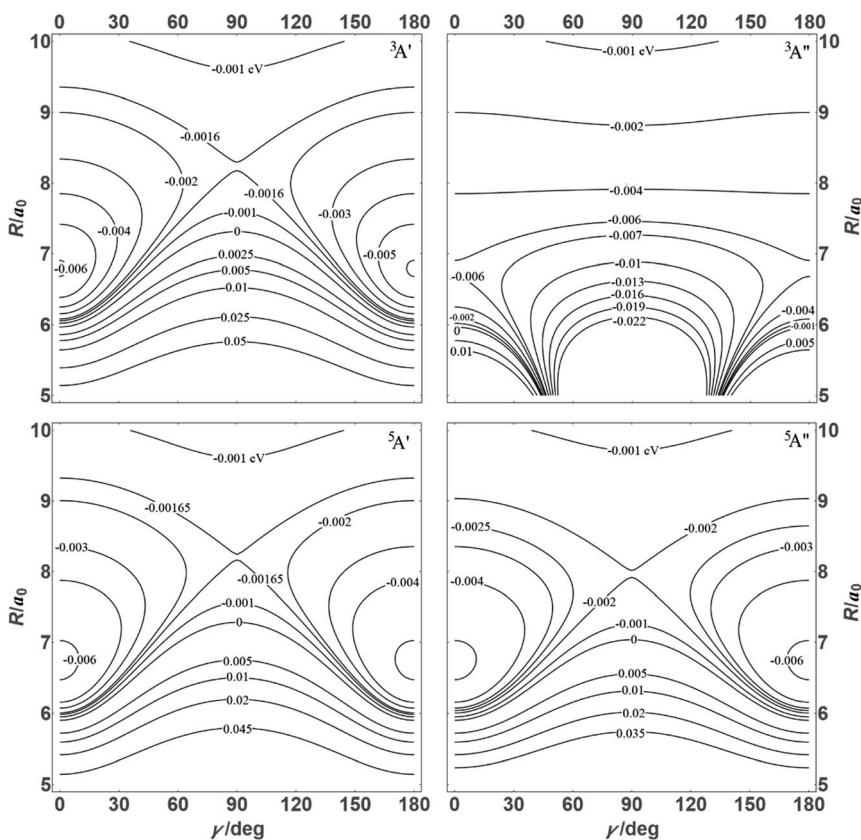

Fig. 3 Energy contours (in eV) of the $^3A'$, $^3A''$, $^5A'$, $^5A''$ states of the N + OH system (coordinates as in Fig. 2).

$$U_{2S+1_{A'}} = a + c_s + b + d_s = U^0_{2S+1_{A'}} + U^2_{2S+1_{A'}} P_2(\cos \theta)$$

$$U_{2S+1_{A''}} = a + c_s - b - d_s = U^0_{2S+1_{A''}} + U^2_{2S+1_{A''}} P_2(\cos \theta)$$

(7)

with a, b, c_S, and d_S as given in eqn (4) and (5). The expressions in eqn (7) have $P_2(\cos \theta)$ – anisotropies such as illustrated in the contour map of Fig. 2 for the $^3A''$ PES (left-hand side of the figure). The present results from asymptotic theory in Fig. 2 are compared with the results from the *ab initio* calculations of ref. 19 (right-hand side of the figure). The general agreement looks satisfactory. Contour plots for the nonreactive $^3A'$, $^5A'$, and $^5A''$ states are compared with those for the reactive $^3A''$ state in Fig. 3.

3. Adiabatic channel potential energy curves and good quantum numbers

Adiabatic channel (AC) potential energy curves $V_i(R)$, for the $^3A''$ electronic state of the N–OH system, are obtained by diagonalization of the Hamiltonian $\hat{H} = \hat{H}^{rot}_{OH} + \hat{U}_{3_{A''}}$ in the basis of rigid rotor functions, where $\hat{U}_{3_{A''}}$ has the asymptotic P_2-anisotropy (see eqn (7)). In an NBO approach, the asymptotic Hamiltonian $\hat{H} = \hat{H}^{rotr}_{OH} + \hat{U}^{ind} + \hat{U}^{disp} + \hat{U}^{ex}_S$ in $\hat{H}^{rotr}_{OH}$, in addition to the rotational Hamiltonian $\hat{H}^{rot}_{OH}$ also includes the spin–orbit (SO) interaction. NBO AC potential energy curves $V_i(R)$ then are obtained by diagonalization of the Hamiltonian in the basis of the functions from eqn (2), multiplied by rotronic functions with the projection Λ of the rotronic momentum K of OH onto its axis. Details of the diagonalization procedure have been described in ref. 2 and will be not repeated here.

The ACs are characterized by sets of good quantum numbers and are specified by indices "i". The ACs lead from those of the separated reactants N + OH into those of the adduct NOH. Conserving total angular momentum (exact quantum number J), and its projection onto the slowly rotating N···O collision axis (good quantum number k, with $k \leq J$), in the BO approximation is of particular importance. Because of too short times for Coriolis mixing, k can be assumed to be conserved during the initial capture and the primary redissociation process. For the present distribution of atomic masses and not too high rotational states of the reactant OH, the orbital angular momentum of the collision pair (quantum number l), is close to the total angular momentum (*i.e.*, $J \approx l$). The states of the free reactant OH are characterized by rotational (neglecting SO) and vibrational quantum numbers $j_{OH} \ll J$ and n_{OH}, respectively. The adduct NOH is represented by a rigid symmetric top (characterized by the quantum numbers J and k) and by three separated Morse oscillators with the vibrational quantum numbers n_1, n_2, and n_3 (spectroscopic parameters were taken from ref. 20 and 27).

In the framework of SACM, the quantum number n_{OH} during the capture and primary redissociation stage of the encounter correlates with the quantum number n_1 of the high-frequency vibration of NOH. Considering low-energy collisions with $n_{OH} = n_1 = 0$ only, we exclude OH stretching transitions during this stage of the process. The quantum number j_{OH} then correlate with the quantum number n_2 of the deformation vibration of the nearly T-shaped adduct NOH, according to a relationship
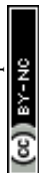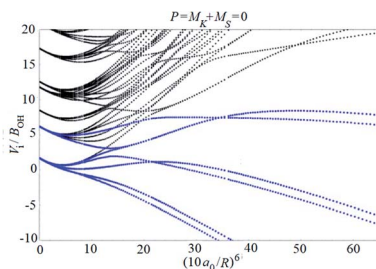
Fig. 4 NBO AC potential energy curves of the N + OH system (curves belonging to the attractive $^3A''$ PES at small intermolecular distances R are drawn in blue, the curves belonging to the repulsive PESs are drawn in black). At large R, all curves correlate with the rotronic states of free OH (only curves corresponding to $P = 0$ are shown).

$$n_2 = j_{OH} - |k| \tag{8}$$

In the NBO approach, the projection of the total momentum J (now including the total spin S of the system) onto the slowly rotating N–O axis is characterized by the good quantum number P (at large intermolecular distances, $P = M_K + M_S$, where M_K and M_S are the respective projections of K and S onto the mentioned axis, see ref. 2).

Examples of rotronic NBO AC potential energy curves are shown in Fig. 4 and 5. At small intermolecular distances R (right-hand side of the figures), the attractive curves (drawn in blue) correlate with the $^3A''$ curves of NOH (with their given k and n_2). At large R (left-hand side of the figures), the NBO curves approach the rotronic states of free OH (with the rotational constant of OH denoted by B_{OH}). NBO AC potential energy curves correlating with BO curves from repulsive PESs (drawn in black) are included in Fig. 4 and 5. As only the attractive $^3A''$ PES leads to reaction, only NBO curves correlating with the corresponding BO ACs are further considered.

The curves show a number of avoided crossings. The passing of the narrowest crossing ($\delta V \leq 0.1 B_{OH}$) is considered as diabatic, see ref. 2 (otherwise it is considered as adiabatic). At short distances ($R < 5a_0$), the degeneracy g_i of the attractive NBO curves correlating with the $(^3A'', k, n_2)$ BO level of NOH is equal to unity when both of P and k are equal to zero, otherwise one has $g_i = 2$.
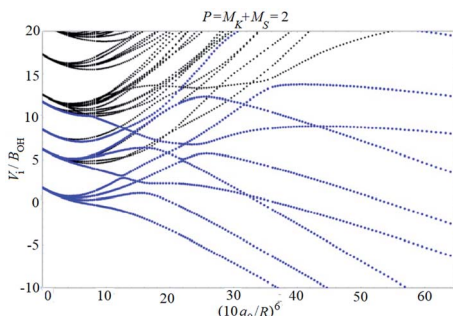

Fig. 5 As Fig. 4, but for $P = 2$.

Table 4 Total angular quantum numbers J_{cl} for closing of incoming (bold numbers) and outgoing (light numbers) ACs on the $^3A''$ PES of NOH (for initial conditions $E_{col} = 0.1$ eV, $n_{OH} = 0$, and $j_{OH} = 10$, NBO effects of SO interaction are neglected)

j_{OH}	$k =$ 0	1	2	3	4	5	6	7	8	9	10	11
11						14	33	42	48	50	52	52
10					25	40	50	57	61	64	66	
9				31	45	55	62	68	72	75		
8			34	48	58	66	72	77	81			
7		36	50	61	69	76	81	86				
6	37	52	63	71	79	84	89					
5	52	64	73	80	87	92						
4	64	74	82	89	94							
3	74	83	90	96								
2	83	90	97									
1	91	98										
0	98											

4. Low-energy cross sections and low-temperature rate constants

The maxima of the sum of the AC potential energy curves $V_i(R)$ and the approximate orbital energies $\hbar J(J + 1)/2 \mu R^2$ of the N$\cdots$OH collision pair define the AC threshold energies $E_{0,i}$ (observing that $l \approx J$). When the energy of the system is larger than $E_{0,i}$, ACs are treated as "open" for capture; otherwise they are "closed". The range of open and closed channels can be characterized by those values J_{cl} at which, for a given collision energy E_{col}, channels with increasing J pass from open to closed. For example, at $E_{col} = 0.1$ eV, $n_{OH} = 0$, $j_{OH} = 10$, and the possible projection quantum numbers k (with $k \leq J$), values for J_{cl} as shown in Table 4 are obtained (line with bold numbers). Once the values of J_{cl} are known, the
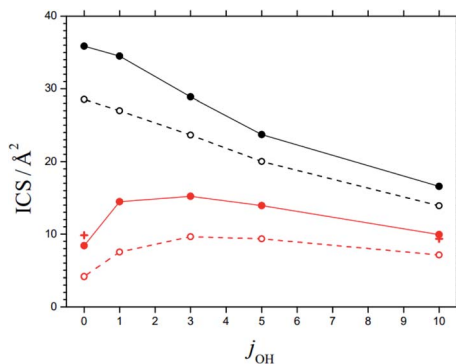
Fig. 6 State-specific cross sections ICS for capture (black) and reaction (red), at $E_{col} = 0.1$ eV (solid curves) and 0.2 eV (dashed curves) and for rotational quantum numbers j_{OH} (curves = statistical theory for the $^3A''$ PES from the present work, red crosses = results for reaction at $E_{col} = 0.1$ eV from the CT calculations of ref. 28, omitting f_{el}, NBO effects of SO interaction are neglected).

corresponding state-specific cross sections ICS_{cap} and rate constants k_{cap} for capture follow as discussed in ref. 2. Fig. 6 shows examples of ICS_{cap} at two collision energies and a variety of j_{OH}.

Overcoming the $E_{0,i}$, however, is not sufficient for reaction. Instead, there may be redissociation of the adducts to the initial reactants, similar to what has been observed in the CT calculations of a reaction between OH and O, see ref. 36–38. One of the aims of the present work was the characterization of this effect by a specific criterion for the formation of randomized states of the adduct. We suggest that two types of redissociation can occur, one during the primary encounter between the reactants before such an adduct is formed, and the other after randomization has taken place. The former we term "primary redissociation", while the latter is called "secondary redissociation". The latter needs an application of unimolecular rate theory and will be elaborated in detail in ref. 39 and 40. Here, the condition for forming randomized adduct states is described in the following. We assume that only that part of the open ACs does not undergo primary redissociation, but succeeds to form long-lived NOH adducts capable for reaction, whose modeled energy levels $E_{NOH}(J, k, n_1, n_2, n_3)$ meet the total energy of the system. Thus, the following conditions must be fulfilled

$$E_{tot} \geq E_{NOH}(J, k, n_1, n_2, n_3) \tag{9a}$$

$$E_{tot} \leq E_{NOH}(J, k + 1, n_1, n_2, n_3) \tag{9b}$$

$$E_{tot} \leq E_{NOH}(J, k, n_1 + 1, n_2, n_3) \tag{9c}$$

$$E_{tot} \leq E_{NOH}(J, k, n_1, n_2 + 1, n_3) \tag{9d}$$

$$E_{tot} \leq E_{NOH}(J, k, n_1, n_2, n_3 + 1) \tag{9e}$$

The total energy E_{tot}, as measured from the bottom of the NOH potential well, is given here by the collision energy E_{col} plus the internal energy of OH. n_1, n_2, and n_3 are the quantum numbers of separated vibrations of NOH, approximated by Morse oscillators. The quantum numbers J and k, for overall angular momentum and its projection, respectively, define the rotational contribution to E_{NOH} in rigid symmetric top approximations. During the approach of N and OH, the quantum numbers n_2 of the adduct form according to the correlation of eqn (8). When the criterion for complex formation of eqn (9) is not fulfilled, there may be a statistical redistribution of n_2 (under conservation of k and n_1) over other ACs correlating with them. j_{OH} then, in general will have changed. For separation of the reactants, the outgoing collision pair (with conserved J and k), however, then will also have to overcome its AC threshold. The corresponding J_{cl} will then differ from the value for the incoming collision pair. Table 4, therefore, includes values of J_{cl} for outgoing collision pairs (lines with light numbers). If the outgoing collision pair does not succeed to overcome its threshold, it tries again by changing n_2 and so on. As the barriers on the way from N + OH to H + NO are considerably lower than the entrance energy in Fig. 1, there is only a limited extent of secondary redissociation under low-energy and low-temperature conditions (contributing to reaction probabilities by a factor of more than 0.9, see ref. 39 and 40). We, therefore, focus our attention here on the primary redissociation only.
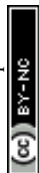
In order to justify the use of the criterion in eqn (9), we have calculated state-specific cross sections ICS for the full reaction (1). For the moment, the results could not be compared with experimental product distributions. However, a comparison with the CT and QS calculations of ref. 24–29 on the $^3A''$ PES showed satisfactory agreement. Fig. 6 illustrates this for an ICS on the $^3A''$ PES as a function of j_{OH} (for collision energies $E_{col} = 0.1$ and 0.2 eV). The agreement of results from the present work and from the CT calculations of ref. 28 is taken as confirmation for the validity of the criterion of eqn (9). The agreement of the ICS for $j_{OH} = 0$ and 10 deserves particular mention.

Accounting for the described primary (and secondary) redissociation, reaction rate constants k_r and reaction probabilities k_r/k_{cap} were determined. This was done by inspecting individual AC potential energy curves and their $E_{0,i}$ values in the framework of BO and NBO treatments. Results from BO calculations were multiplied with the electronic factor $f_{el}(T)$, in the present case given by

$$f_{el}(T) = 3/(8 + 8 \exp[-205 \text{ K}/T]) \tag{10}$$

Fig. 7 shows the results. Between 50 and 200 K, the BO rate constants practically agree with the experimental data and NBO effects do not yet play a major role. However, in contrast to the $k_{cap}(T)$, BO and NBO results for reaction rate constants k_r below about 50 K differ markedly. NBO couplings, relevant for low-temperature conditions, here efficiently loosen the restrictions imposed by eqn (9) and in this way partly circumvent redissociation effects. On the one hand, this illustrates the importance of NBO effects under low-temperature conditions. On the other hand, the close agreement between calculations and experiments between 50 and 200 K also validates the criterion of eqn (9) for formation of randomized intermediate adducts capable of reaction.

Compared to the $f_{el}(T)$-corrected BO results, the NBO calculations of capture rate constants $k_{cap}(T)$ led to only slightly larger limiting low-temperature values. The results obtained practically agreed with those from the ACCSA calculations of ref. 23. The low-temperature region accordingly is governed by the long-range dispersion and induction contributions only, while short-range exchange contributions will become relevant only at higher collision energies. The near-
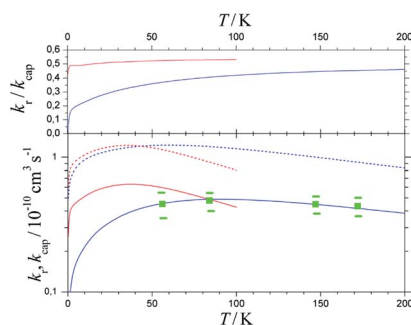

Fig. 7 Reaction probabilities k_r/k_{cap} (upper panel), capture rate constants k_{cap} (lower panel, dashed curves) and reaction rate constants k_r (lower panel, solid curves), from $f_{el}(T)$-corrected BO (blue curves) and NBO (red curves) calculations of the present work, in comparison to experimental results from ref. 33 (green symbols with error bars).
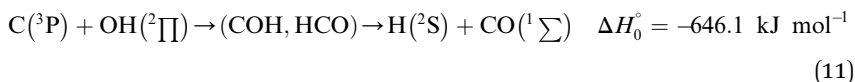
agreement of the present $k_{cap}(T)$ with the results from the ACCSA and SACM treatments of ref. 23 is not surprising. It has been shown in ref. 34 that the two approaches, as well as "adiabatic variance" or "perturbed rotational state" treatments such as employed in ref. 43 and 44, are equivalent and small differences arise from numerical differences only.
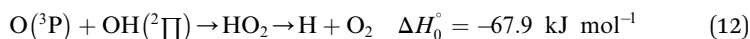
As the number of considered ACs for technical reasons was limited, only calculations for low temperatures were made in the present work. However, the comparison with the experimental rate constants k_r from ref. 33 in Fig. 7 appears satisfactory. It leads to reaction probabilities k_r/k_{cap} of the order of 1/2, which are consistent with the values empirically suggested in ref. 23. Although the present study was limited to low temperatures, according to Fig. 7 it does not appear improbable to assume only a weak temperature dependence above 200 K. The results from the present work on the one hand illustrate the importance of NBO effects under low-temperature conditions. On the other hand, the close agreement between calculations and experiments validates the criterion of eqn (12) and (13) for formation of randomized intermediate adducts capable of reaction.
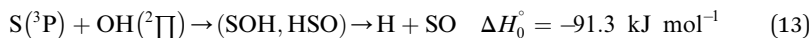
5. Discussion

A comparison of the results for reaction (1) with related information for other reactions leads to interesting conclusions. This appears most clear for the reaction

$$C(^3P) + OH(^2\textstyle\prod) \rightarrow (COH, HCO) \rightarrow H(^2S) + CO(^1\textstyle\sum) \quad \Delta H_0^\circ = -646.1 \text{ kJ mol}^{-1}$$

$$(11)$$

which involves analogous intrinsic dynamics of the primary adduct to that shown in Fig. 1.[45,46] In comparison to reaction (1), reaction (11) is far more exothermic and the primary adduct COH is formed with larger vibrational excitation ($C(^3P)$ + $OH(^2\Pi)$ → COH with $\Delta H_0^\circ = -531$ kJ mol^{-1} in contrast to $N(^4S)$ + $OH(^2\Pi)$ → NOH with $\Delta H_0^\circ = -300$ kJ mol^{-1}). In contrast to that of reaction (1), the overall rate constant for reaction (11) was found to be close to the capture rate constant,[47] i.e. neither primary nor secondary redissociation were found to play a significant role. In view of the large endothermicity of a process (COH, HCO) → C + OH this is not surprising for secondary redissociation, but primary redissociation caused by the conditions in eqn (9) apparently is also not too important. As the vibrational frequencies of the adducts are not very different, the reason must be a much larger density of vibrational adduct states in reaction (11) which allow the condition of eqn (9) to be fulfilled more easily. The chance of hitting an adduct state by the capture process then is much larger in reaction (11) than in reaction (1) which reduces the probability for primary redissociation. The reactions

$$O(^3P) + OH(^2\textstyle\prod) \rightarrow HO_2 \rightarrow H + O_2 \quad \Delta H_0^\circ = -67.9 \text{ kJ mol}^{-1} \quad (12)$$

and

$$S(^3P) + OH(^2\textstyle\prod) \rightarrow (SOH, HSO) \rightarrow H + SO \quad \Delta H_0^\circ = -91.3 \text{ kJ mol}^{-1} \quad (13)$$

(with adduct energies corresponding to O + OH → HO$_2$, $\Delta H_0^\circ = -248.1$ kJ mol^{-1}, or S + OH → HOS, $\Delta H_0^\circ = -315.9$ kJ mol^{-1}, respectively) like reaction (1) were

found to have reaction probabilities as low as 1/2. As the exothermicities of these reactions are markedly different from that of reaction (11), the distinction between primary and secondary redissociation is more difficult. The situation may be comparable to that of reaction (1) with a primary redissociation characterized by the criterion of eqn (9), but secondary redissociation also has to be considered here.

Adducts with larger vibrational densities of states have a larger chance to fulfill the criterion of eqn (9a)–(9e) during the capture process. Primary redissociation, therefore, appears to be a phenomenon encountered in reaction systems of limited complexity only. The reactions mentioned in the introduction, with experimental rate constants equal to the capture rate constants, apparently do not fall into this category. Obviously, for reactions without adduct formation, primary redissociation appears less probable.

A comparison of the present results with the work of ref. 2 on reaction (11) also sheds light on the role of NBO effects in low-temperature rate constants. With a single attractive PES contributing to product formation, reaction (1) shows only small NBO effects on the capture rate constants. On the other hand, CT and NBO calculations for reaction (11), where primary redissociation apparently can be neglected, have led to similar limiting low-temperature rate constants as long as only capture on the lowest PES was important (up to about 20 K, where k_{cap} rises by about a factor of 2 from its low-temperature limiting value). Between 20 and 200 K, however, k_{cap} in the lowest electronic state of the adduct was found to be successively replaced by capture into higher electronic states, with an overall rate constant not varying too much with temperature. Obviously, NBO effects play an important role there.

In summary, the comparison of the N + OH with the C + OH reaction identifies differences in the role of primary redissociation effects during adduct formation. Further differences arise from different numbers of attractive electronic states of the adducts. The present work highlights the application of statistical rate theories and their extension by the conditions of eqn (9) to reaction (1). In this way, we rationalize the results from CT and CS calculations.

Conflicts of interest

There are no conflicts to declare.

References

1 J. Troe, Simplified representation of partial and total rate constants of complex-forming bimolecular reactions, *J. Phys. Chem. A*, 2015, **119**, 12159–12165.

2 A. I. Maergoiz, E. E. Nikitin and J. Troe, Electronic nonadiabatic effects in low temperature radical-radical reactions. I. C(^{3}P) + OH(X$^2\Pi$), *J. Chem. Phys.*, 2014, **141**, 044302.

3 A. I. Maergoiz, E. E. Nikitin, J. Troe and V. G. Ushakov, Asymptotic interaction between open shell partners operative in low-temperature complex formation: H(^{2}S) + O$_2$(X$^3\Sigma_g^-$) and O(^{3}P) + OH($^2\Pi$) systems, in *Theory of chemical reaction dynamics*, NATO ASI Series, ed. G. Lendvay, Kluwer, Dordrecht, 2004, pp. 21–44.

4 M. M. Graff and A. F. Wagner, Theoretical studies of fine-structure effects and long-range forces: Potential energy surfaces and reactivity of O(^{3}P) + OH(^{2}Π), *J. Chem. Phys.*, 1990, **92**, 2423–2439.

5 A. Potapov, A. Canosa, E. Jiménez and B. Rowe, Uniform supersonic chemical reactors: 30 years of astrochemical history and future challenges, *Angew. Chem., Int. Ed.*, 2017, **56**, 8618–8640.

6 K. M. Hickson and A. Bergeat, Low temperature kinetics of unstable radical reactions, *Phys. Chem. Chem. Phys.*, 2012, **14**, 12057–12069.

7 M. Quack and J. Troe, Specific rate constants of unimolecular processes II.Adiabatic channel model, *Ber. Bunsen-Ges. Phys. Chem.*, 1974, **78**, 240–252.

8 M. Quack and J. Troe, Complex formation in reactive and inelastic scattering: Statistical Adiabatic Channel Model of unimolecular processes III, *Ber. Bunsen-Ges. Phys. Chem.*, 1975, **79**, 170–183.

9 A. I. Maergoiz, E. E. Nikitin, J. Troe and V. G. Ushakov, Classical trajectory and adiabatic channel study of the transition from adiabatic to sudden capture dynamics. I. Ion - dipole capture, *J. Chem. Phys.*, 1996, **105**, 6263–6269.

10 A. I. Maergoiz, E. E. Nikitin, J. Troe and V. G. Ushakov, Classical trajectory and adiabatic channel study of the transition from adiabatic to sudden capture dynamics. II. Ion - quadrupole capture, *J. Chem. Phys.*, 1996, **105**, 6270–6276.

11 A. I. Maergoiz, E. E. Nikitin, J. Troe and V. G. Ushakov, Classical trajectory and adiabatic channel study of the transition from adiabatic to sudden capture dynamics. III. Dipole - dipole capture, *J. Chem. Phys.*, 1996, **105**, 6263–6269.

12 A. I. Maergoiz, E. E. Nikitin, J. Troe and V. G. Ushakov, Classical trajectory and statistical adiabatic channel study of the dynamics of capture and unimolecular bond fission. IV. Valence interactions between atoms and molecules, *J. Chem. Phys.*, 1998, **108**, 5265–5280.

13 A. I. Maergoiz, E. E. Nikitin, J. Troe and V. G. Ushakov, Classical trajectory and statistical adiabatic channel study of the dynamics of capture and unimolecular bond fission. V. Valence interactions two linear rotors, *J. Chem. Phys.*, 1998, **108**, 9987–9998.

14 E. I. Dashevskaya, I. Litvin, E. E. Nikitin and J. Troe, Modelling low-energy electron-molecule capture processes, *Phys. Chem. Chem. Phys.*, 2008, **10**, 1270–1276.

15 F. Pauzat, Y. Ellinger, G. Berthier, M. Gérin and Y. Viala, Theoretical study of a basic process in interstellar nitrogen chemistry: reaction of N with OH, *Chem. Phys.*, 1993, **174**, 71–79.

16 M. Stumpf, A. J. Dobbyn, D. H. Mordaunt, H.-M. Keller, H. Flöthmann, R. Schinke, H.-J. Werner and K. Yamashita, Unimolecular dissociations of HCO, HNO, and HO$_2$: From regular to irregular dynamics, *Faraday Discuss.*, 1995, **102**, 192–213.

17 R. Guadagnini, G. C. Schatz and S. P. Walch, Global potential energy surfaces for the lowest ^{1}A′, ^{3}A″, and ^{1}A″ states of HNO, *J. Chem. Phys.*, 1995, **102**, 774–783.

18 D. H. Mordaunt, H. Flöthmann, M. Stumpf, H.-M. Keller, C. Beck, R. Schinke and K. Yamashita, The dissociation of HNO. I. Potential energysurfaces for the X ^{1}A', A ^{1}A'', and a ^{3}A'' states, *J. Chem. Phys.*, 1997, **107**, 6603–6615.

19 A. Li, C. Xie, D. Xie and H. Guo, A global *ab initio* potential energy surface for HNO (a^{3}A″) and quantum mechanical studies of vibrational states and reaction dynamics, *J. Chem. Phys.*, 2011, **134**, 194309.
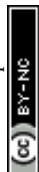
20 U. Bozkaya, J. M. Turney, Y. Yamaguchi and H. F. Schaefer, The lowest electronic singlet and triplet potential energy surfaces for the HNO – NOH system: Energetics, unimolecular rate constants, tunneling and kinetic isotope effects for the isomerization and dissociation reactions, *J. Chem. Phys.*, 2012, **136**, 164303.

21 C. J. Cobos, Theoretical analysis of the rate constants for the interstellar reaction N + OH → NO + H, *Int. J. Chem. Kinet.*, 1995, **27**, 219–233.

22 D. Edvardsson, C. F. William and D. C. Clary, Rate constant calculations on the N(^{4}S) + OH (X$^2\Pi$) reaction, *Chem. Phys. Lett.*, 2006, **431**, 261–266.

23 T. Stoecklin, B. Bussery-Honvault, P. Honvault and F. Dayou, Asymptotic potentials and rate constants in the adiabatic capture centrifugal sudden approximation for X + OH(X$^2\Pi$) → OX + H(^{2}S) reactions where X = O(^{3}P), S(^{3}P) or N(^{4}S), *Comput. Theor. Chem.*, 2012, **990**, 39–46.

24 R. Guadagnini, G. C. Schatz and S. P. Walch, Quasiclassical trajectory studies of N + OH, O + NH, and H + NO collisions using global *ab initio* potential energy surfaces, *J. Chem. Phys.*, 1995, **102**, 784–791.

25 M. Jorfi, P. Honvault and P. Halvick, Quasi-classical determination of integral cross-sections and rate constants for the N + OH → NO + H reaction, *Chem. Phys. Lett.*, 2009, **471**, 65–70.

26 M. Jorfi, P. Honvault and P. Halvick, Quasiclassical trajectory calculations of differential cross sections and product energy distributions for the N + OH → NO + H reaction, *J. Chem. Phys.*, 2009, **131**, 094302.

27 C. Xie, A. Li, D. Xie and H. Guo, State-to-state quantum dynamics of the N(^{4}S) + OH (X$^2\Pi$) → H(^{2}S) + NO (X$^2\Pi$) reaction, *J. Chem. Phys.*, 2011, **135**, 164312.

28 N. Bulut, O. Roncero, M. Jorfi and P. Honvault, Accurate time dependent wave packet calculations for the N + OH reaction, *J. Chem. Phys.*, 2011, **135**, 104307.

29 X. Hu, C. Xie and D. Xie, State-to-state reaction dynamics for the reaction of atom N with radicals, *Int. J. Quantum Chem.*, 2015, **115**, 596–606.

30 M. J. Howard and I. W. M. Smith, Direct rate measurements on the reactions N + OH →NO + H and O + OH →O$_2$ + H from 250 to 515 K, *J. Chem. Soc., Faraday Trans. 2*, 1981, **77**, 997–1008.

31 W. H. Brune, J. J. Schwab and J. G. Anderson, Laser magnetic resonance, resonance fluorescence, and resonance absorption studies of the reactions O + OH →O$_2$ + H, O + HO$_2$ →OH + O$_2$, N + OH →NO + H, and N + HO$_2$ → products at 300 K between 1 and 5 torr, *J. Phys. Chem.*, 1983, **87**, 4503–4514.

32 I. W. M. Smith and D. W. A. Stewart, Low-temperature kinetics and reactions between neutral free radicals. Rate constants for the reactions of OH radicals with N atoms (103 ≤T/K ≤294) and with O atoms (158 ≤T/K ≤294), *J. Chem. Soc., Faraday Trans.*, 1994, **90**, 3221–3227.

33 J. Daranlot, M. Jorfi, C. Xie, A. Bergeat, M. Costes, P. Caubet, D. Xie, H. Guo, P. Honvault and K. M. Hickson, Revealing atom-radical reactivity at low temperature through the N + OH reaction, *Science*, 2011, **334**, 1538–1541.

34 M. L. Dubernet and R. McCarroll, Rotational state dependence of ion-polar molecule reactions at very low temperature, *Z. Phys. D: At., Mol. Clusters*, 1989, **13**, 255–258.

35 J. Troe, Statistical adiabatic channel model for ion-molecule capture processes. II. Analytical treatment of ion-dipole capture, *J. Chem. Phys.*, 1996, **105**, 6249–6262.

36 J. A. Miller, Nonstatistical effects and detailed balance in quasiclassical trajectory calculations of the thermal rate coefficient for O + OH $\rightarrow$O$_2$ + H, *J. Chem. Phys.*, 1986, **84**, 6170–6177.

37 G. Nyman and J. Davidsson, A low-energy quasiclassical trajectory study of O(^{3}P) + OH($^2\Pi$) $\rightarrow$ O$_2$($^3\Sigma_g^-$)+ H(^{2}S)". II. Rate constants and recrossing, zero-point energy effects, *J. Chem. Phys.*, 1990, **92**, 2415–2422.

38 G. Nyman, Dynamical and statistical behaviour of O(^{3}P) + OH($^2\Pi$) $\rightarrow$ H(^{2}S) + O$_2$($^3\Sigma_g^-$), *Chem. Phys.*, 1993, **173**, 159–66.

39 A. I. Maergoiz, E. E. Nikitin and J. Troe, Statistical interpretation of rate constants for the reaction N + OH $\rightarrow$NO + H. I. Thermal rate constants, *J. Chem. Phys.*, to be submitted.

40 A. I. Maergoiz, E. E. Nikitin and J. Troe, Statistical interpretation of rate constants for the reaction N + OH $\rightarrow$NO + H. II. Product energy distributions, *J. Chem. Phys.*, to be submitted.

41 E. Goos, A. Burcat and B. Ruscic, *Extended Third Millennium Ideal Gas and Condensed Phase Thermochemical Database for Combustion with Updates from Active Thermochemical Tables*, http://burcat.technion.ac.il/div September 2005, January 2015.

42 E. E. Nikitin and S. Ya. Umanskii, *Theory of slow atomic collisions*, Springer Series in Chemical Physics, Springer-Verlag Berlin, New York, 1984, vol. 30.

43 K. Sakimoto and K. Takayanagi, Influence of the dipole orientation on the low-energy ion-molecule reactions, *J. Phys. Soc. Jpn.*, 1980, **48**, 2076–2083.

44 D. R. Bates, Ion-polar molecule encounters, *Proc. R. Soc. London, Ser. A*, 1982, **384**, 289–300.

45 A. Zanchet, B. Bussery-Honvault, M. Jorfi and P. Honvault, C(^{3}P) + OH(X$^2\Pi$) $\rightarrow$ CO(a$^3\Pi$) + H(^{2}S) reaction: fully global *ab initio* energy surfaces of the 1^{2}A$''$ and 1^{4}A$''$ excited states and non adiabatic couplings, *Phys. Chem. Chem. Phys.*, 2009, **11**, 6182–6191.

46 M. Jorfi, T. González-Lezana, A. Zanchet, P. Honvault and B. Bussery-Honvault, Quasiclassical trajectoryand statistical quantum calculations for the C + OH $\rightarrow$CO + H reaction on the first excited 1^{2}A$''$ potential energy surface, *J. Phys. Chem. A*, 2013, **117**, 1872–1879.

47 M. Jorfi, B. Bussery-Honvault, P. Honvault, T. Stoecklin, P. Larrégaray and P. Halvick, Theoretical sensitivity of the C(^{3}P) + OH(X$^2\Pi$) $\rightarrow$ CO(X$^1\Sigma^+$) + H(^{2}S) rate constant: The role of the long-range potential, *J. Phys. Chem. A*, 2010, **114**, 7494–7499.